

THE NATURE OF THE HYPER-RUNAWAY CANDIDATE HIP 60350^{1,2}

ANDREAS IRRGANG³, NORBERT PRZYBILLA³, ULRICH HEBER³, M. FERNANDA NIEVA^{4,5} AND SONJA SCHUH^{6,7}
Draft version November 17, 2018

ABSTRACT

Young, massive stars in the Galactic halo are widely supposed to be the result of an ejection event from the Galactic disk forcing some stars to leave their place of birth as so-called runaway stars. Here, we present a detailed spectroscopic and kinematic analysis of the runaway B-star HIP 60350 to determine which runaway scenario – a supernova explosion disrupting a binary system or dynamical interaction in star clusters – may be responsible for HIP 60350’s peculiar orbit. Based on a non-local thermodynamic equilibrium approach, a high-resolution optical echelle spectrum was examined to revise spectroscopic quantities and for the first time to perform a differential chemical abundance analysis with respect to the B-type star 18 Peg. The results together with proper motions from the *Hipparcos* Catalog further allowed the three-dimensional kinematics of the star to be studied numerically. The abundances derived for HIP 60350 are consistent with a slightly supersolar metallicity agreeing with the kinematically predicted place of birth ~ 6 kpc away from the Galactic center. However, they do not exclude the possibility of an α -enhanced abundance pattern expected in the case of the supernova scenario. Its outstanding high Galactic rest frame velocity of 530 ± 35 km s⁻¹ is a consequence of ejection in the direction of Galactic rotation and slightly exceeds the local Galactic escape velocity in a standard Galactic potential. Hence HIP 60350 may be unbound to the Galaxy.

Subject headings: stars: abundances — stars: atmospheres — stars: distances — stars: early-type — stars: individual (HIP 60350, 18 Peg) — stars: kinematics and dynamics

1. INTRODUCTION

Young, massive stars at high galactic latitudes are rare objects albeit known for decades (Blaauw 1961). According to Tobin (1987), there are several plausible alternatives to explain them. The possibilities encompass I) *in situ* star formation caused by the collision of intermediate or high-velocity H I clouds, II) misinterpretation of rather hot evolved stars closely mimicking massive ones or III) the formation in the disk and subsequent ejection into the halo as so-called runaway stars. Possible ejection scenarios for the latter are dynamical interaction in star clusters – either initial dynamical relaxation (Poveda et al. 1967) or many-body encounters (Leonard & Duncan 1988) – or a supernova explosion in a binary system (Blaauw 1961).

Interest in runaway stars has been revived recently by the discovery of a new class of extreme velocity stars (Brown et al. 2005; Edelmann et al. 2005; Hirsch et al.

2005), the so-called hypervelocity stars (HVSs), traveling at such a high velocity that they escape from the Galaxy. They were first predicted by theory (Hills 1988) to be the result of the tidal disruption of a binary system by a supermassive black hole (SMBH) that accelerates one component to beyond the Galactic escape velocity (the Hills mechanism). Because the Galactic center hosts such a SMBH it is the suggested place of origin for HVSs. However, the SMBH paradigm has been challenged recently by the young HVS HD 271791 because its kinematics point to a birthplace in the metal-poor rim of the Galactic disk (Heber et al. 2008). Przybilla et al. (2008b) presented a high-precision quantitative spectral analysis and conclude that HD 271791 is the surviving secondary of a massive binary system disrupted in a supernova explosion. A similar scenario has been proposed for the origin of runaway B stars by Blaauw (1961); hence, Przybilla et al. coined the term hyper-runaway star for the most extreme runaways that exceed the Galactic escape velocity.

HIP 60350 is a bright ($V = 11.60$ mag; Tobin 1985) mid-B-type star of high Galactic latitude ($l = 144.6^\circ, b = +75.1^\circ$). Among others, the star was extensively studied by Maitzen et al. (1998) who estimated its atmospheric parameters from photometric indicators: effective temperature $T_{\text{eff}} = 17\,100$ K and logarithmic surface gravity $\log(g [\text{cm s}^{-2}]) = 4.3$, and they derived the radial velocity to $v_{\text{rad}} = 217 \pm 20$ km s⁻¹. Moreover, they inferred a distance of 3.5 kpc, a mass of $5 M_\odot$ and an age of about 15 Myr. Tenjes et al. (2001) used these values together with *Hipparcos* proper motions to trace back the orbit of HIP 60350 to show that a dynamical disk runaway event 20 Myr ago is very likely the ejection mechanism in this case.

HIP 60350 has a total velocity referred to the

¹ Based on observations obtained with the Hobby-Eberly Telescope, which is a joint project of the University of Texas at Austin, the Pennsylvania State University, Stanford University, Ludwig-Maximilians-Universität München, and Georg-August-Universität Göttingen (proposal G09-1-002).

² Based on observations collected at the Centro Astronómico Hispano Alemán (CAHA) at Calar Alto, operated jointly by the Max-Planck Institut für Astronomie and the Instituto de Astrofísica de Andalucía (CSIC) (proposals H2005-2.2-016, F2009-3.5-008 and H2009-3.5-028).

³ Dr. Karl Remeis Observatory & ECAP, University of Erlangen-Nuremberg, Sternwartstrasse 7, D-96049 Bamberg, Germany; andreas.irrgang@sternwarte.uni-erlangen.de.

⁴ Visiting scientist at the Dr. Karl Remeis Observatory.

⁵ Max Planck Institute for Astrophysics, Karl-Schwarzschild-Strasse 1, D-85741 Garching, Germany.

⁶ Georg-August-Universität Göttingen, Institute for Astrophysics, Friedrich-Hund-Platz 1, 37077 Göttingen, Germany.

⁷ TEA Visiting Professor, Institut für Astronomie und Astrophysik, Kepler Center for Astro and Particle Physics, Eberhard-Karls-Universität, Sand 1, 72076 Tübingen.

TABLE 1
STELLAR PARAMETERS AND ELEMENTAL ABUNDANCES OF HIP 60350 AND 18 PEG

Stellar parameters			$\log(X/H) + 12$		
	HIP 60350	18 Peg	Element	HIP 60350	18 Peg
T_{eff} [K]	$16\,100 \pm 500$	$15\,800 \pm 200$	He	11.21	10.99
$\log(g)$ [cm s^{-2}]	4.10 ± 0.15	3.75 ± 0.05	C	8.79 ± 0.20	8.33 ± 0.09
ξ [km s^{-1}]	5 ± 2	4 ± 1	N	8.20 ± 0.30	7.80 ± 0.11
$v \sin(i)$ [km s^{-1}]	150 ± 5	15 ± 3	O	8.95 ± 0.20	8.80 ± 0.11
ζ [km s^{-1}]	...	10 ± 3	Mg	7.38 ± 0.20	7.51 ± 0.07
v_{rad} [km s^{-1}]	262 ± 5	-14 ± 1	Si	7.66 ± 0.20	7.51 ± 0.11
T_{evol} [Myr]	45^{+15}_{-30}	61 ± 5	S	7.38 ± 0.20	7.08 ± 0.11
d [pc]	3100 ± 600	362 ± 21	Fe	7.18 ± 0.25	7.54 ± 0.07
M/M_{\odot}	4.9 ± 0.2	5.6 ± 0.2			
R/R_{\odot}	2.8 ± 0.2	5.2 ± 0.3			
$\log(L/L_{\odot})$	3.3 ± 0.6	3.2 ± 0.1			

NOTE. — The abundances are averages over all investigated lines of a chemical element. Since only one strong or a few weak lines were available for most elements when considering HIP 60350, conservative abundance uncertainties were estimated by visual inspection (see Fig. 1) instead of using the rms uncertainties from Table 2 as in the case of 18 Peg. The macroturbulent velocity ζ is not measurable for HIP 60350 due to its large $v \sin(i)$.

local standard of rest (LSR) of $v_{\text{LSR}} = 417 \text{ km s}^{-1}$ (Maitzen et al. 1998) making it the second fastest runaway star after the massive B-type giant HD 271791. The various similarities between both stars were motivation to us to re-investigate the origin of HIP 60350.

To this aim we carried out a quantitative analysis of a high-resolution spectrum using non-local thermodynamic equilibrium (NLTE) techniques for the first time. Stellar parameters were thus revised and elemental abundances constrained (Sect. 2). The results together with proper motions from the new reduction of the *Hipparcos* Catalog were used to determine the current three-dimensional (3D) space velocity. The following kinematic analysis suggested that the star originated in or near the Crux-Scutum spiral arm (Sect. 3). Finally we discuss the kinematic parameters and the elemental abundance pattern in the light of the rivaling formation scenarios, i.e., binary supernova versus dynamical cluster ejection (Sect. 4).

2. SPECTROSCOPIC ANALYSIS

HIP 60350 was observed in 2008 December with the high-resolution echelle spectrograph of the 9.2 m Hobby-Eberly Telescope (HET) at the McDonald Observatory. Three individual spectra with resolving power $\lambda/\Delta\lambda = 15\,000$ and useful wavelength range [3900 Å, 7870 Å] were co-added, resulting in a signal-to-noise ratio (S/N) around 140 in the blue visual range. Additionally, three intermediate-resolution spectra taken in 2009 May and July with the 3.5 m telescope at Calar Alto, Spain, and its long-slit TWIN spectrograph were available enlarging the spectral coverage down to 3500 Å, making accessible the high-order Balmer lines and the Balmer jump.

The quantitative spectral analysis was carried out following the hybrid NLTE approach discussed by Nieva & Przybilla (2006, 2007, 2008) and Przybilla et al. (2006): line-blanketed LTE model atmospheres were computed with ATLAS9 (Kurucz 1993), while NLTE line formation calculations were performed using updated versions of DETAIL and SURFACE (Giddings 1981; Butler & Giddings 1985). State-of-the-art model atoms were adopted allowing absolute elemental abundances to be obtained with high accuracy (see Przybilla et al. 2008a,b for an overview). Atmospheric parameters and elemental abundances were derived by detailed line-profile analysis and fitting of the spectral energy distri-

bution (SED).

The fundamental atmospheric parameters $T_{\text{eff}} = 16\,100 \pm 500 \text{ K}$ and $\log(g) = 4.10 \pm 0.15$, microturbulent velocity $\xi = 5 \pm 2 \text{ km s}^{-1}$ and projected rotational velocity $v \sin i = 150 \pm 5 \text{ km s}^{-1}$ were primarily constrained from Balmer and He I lines as well as the Si II/III ionization equilibrium. Elemental abundances were then obtained by matching the measurable lines of the individual chemical species while keeping all other stellar parameters fixed (see Fig. 1). In the end, a final synthetic spectrum was computed which excellently reproduces the observation (see Fig. 2), confirming the B-type nature of HIP 60350. Interestingly, a helium abundance higher than solar, $\log(\text{He}/\text{H}) + 12 = 11.21$, was required to match the helium lines, the depth of the Balmer lines and the SED simultaneously (see Fig. 3). The resulting abundances (averaged over all lines of an element) are listed in Table 1.

All spectra yielded a barycentric radial velocity of $v_{\text{rad}} = +262 \pm 5 \text{ km s}^{-1}$, equivalent to $v_{\text{rad,LSR}} = +268 \pm 5 \text{ km s}^{-1}$ in very good agreement with de Boer et al. (1988) who found $v_{\text{rad,LSR}} = +270 \text{ km s}^{-1}$. Bearing in mind the different time intervals between each measurement, the star is unlikely a binary.

Comparing the location of HIP 60350 in the ($T_{\text{eff}}, \log g$) diagram to evolutionary tracks (Schaller et al. 1992) of solar metallicity as shown in Fig. 4 allowed its mass $M = 4.9 \pm 0.2 M_{\odot}$ and age $T_{\text{evol}} = 45^{+15}_{-30} \text{ Myr}$ to be constrained. The distance to HIP 60350 could then be calculated from M , V , T_{eff} , $\log g$ and extinction $A_V = 3.1 E(B - V) = 0.07 \text{ mag}$ using the method described by Ramspeck et al. (2001) to be $d = 3.1 \pm 0.6 \text{ kpc}$.

The precision of the analysis was restricted by an interplay of three effects: I) HIP 60350 lies in a temperature region where the optical spectrum shows very few strong but many weak metal lines. II) A considerable fraction of the latter is smeared out due to the high projected rotational velocity $v \sin i$. III) The S/N of the available spectra is often not sufficient to accurately determine the continuum behavior. Therefore, only few lines (in the case of magnesium and iron just one, see Table 2) are above the noise level and thus usable.

In order to exclude the possibility that the few lines measurable for HIP 60350 give abundances that are systematically higher or lower than other lines of the same

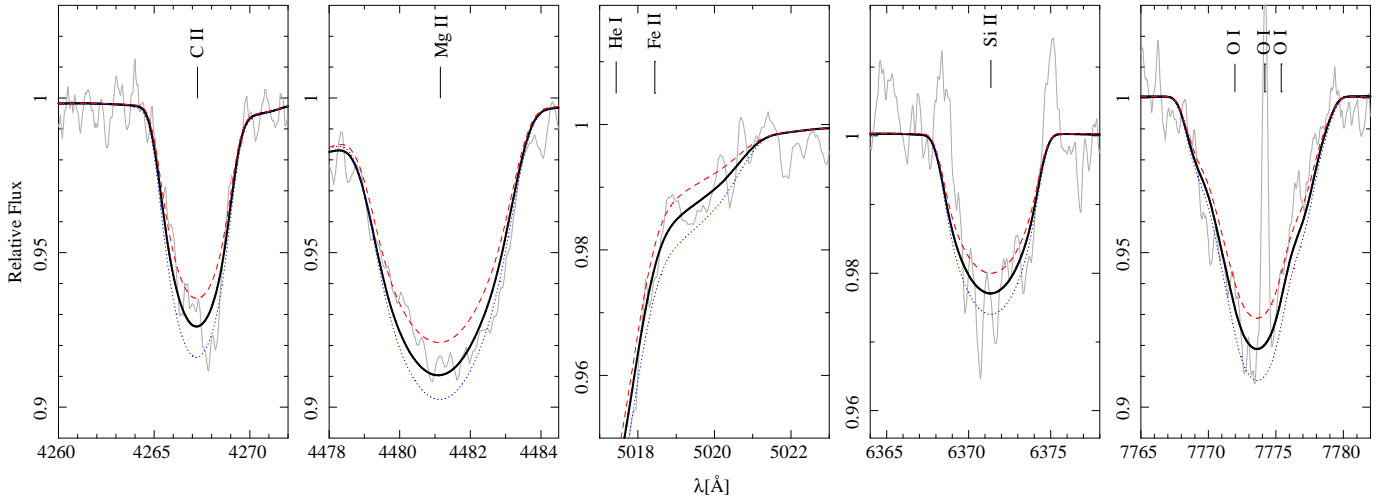


FIG. 1.— Determination of abundances and their uncertainties demonstrated in the cases of C, Mg, Fe, Si and O: the HET observation (gray solid line) is fitted best by the parameters of Table 1 (thick black line). The corresponding uncertainties are deduced visually by varying the abundance of an individual chemical species while keeping all others fixed. Blue dotted/red dashed lines stand for an increase/decrease of abundance according to the uncertainties in Table 1.

TABLE 2
SPECTRAL LINE ANALYSIS OF HIP 60350 AND 18 PEG

$\lambda(\text{\AA})$	$\chi(\text{eV})$	$\log gf$	Accuracy	Source	$\log(X/H) + 12$	
					HIP 60350	18 Peg
C II:						
3918.98	16.33	-0.533	B	WFD	...	8.19
3920.69	16.33	-0.232	B	WFD	...	8.30
4267.00	18.05	0.563	C+	WFD	8.69	8.19
4267.26	18.05	0.716	C+	WFD	"-	"-
4267.26	18.05	-0.584	C+	WFD	"-	"-
5132.94	20.70	-0.211	B	WFD	8.93	8.37
5133.28	20.70	-0.178	B	WFD	"-	"-
5145.16	20.71	0.189	B	WFD	8.73	8.34
5151.09	20.71	-0.179	B	WFD	...	8.39
5662.47	20.71	-0.249	B	WFD	...	8.41
6578.05	14.45	-0.087	C+	N02	...	8.25
6582.88	14.45	-0.388	C+	N02	...	8.37
6783.90	20.71	0.304	B	WFD	...	8.44
					8.79	8.33
					± 0.13	± 0.09

NOTE. — The table for all elements is available at the end of this paper. Accuracy indicators – uncertainties within: A: 3%; B: 10%; C: 25%; D: 50%; E: larger than 50%; X: unknown. Sources of gf -values – BB89: Becker & Butler (1989); BMZ: Butler et al. (1993); FFT: Froese Fischer & Tachiev (2004); FFTI: Froese Fischer et al. (2006); FMW: Fuhr et al. (1988); FW: Fuhr & Wiese (1998); KB: Kurucz & Bell (1995); MAR: Mar et al. (2000); MELZ: Mendoza et al. (1995); MERLR: Matheron et al. (2001); N02: Nahar (2002); N86: Nussbaumer (1986); WFD: Wiese et al. (1996); WSM: Wiese et al. (1969).

chemical species, we also carried out an abundance analysis of the normal Population I B-type star 18 Peg. We used the Fibre Optics Cassegrain Echelle Spectrograph (FOCES; Pfeiffer et al. 1998) on the 2.2 meter telescope at Calar Alto, Spain, to obtain a high-resolution, high-S/N spectrum ($\lambda/\Delta\lambda \approx 40\,000$, $S/N \approx 400$ in the blue) of 18 Peg. Due to the high quality of the spectrum and the establishment of four ionization equilibria, atmospheric parameters and abundances could be constrained with high accuracy (see Fig. 2 for a comparison of the final synthetic spectrum with observation). This particular star was chosen since its parameters are similar to HIP 60350 (see Table 1). Its chemical composition is representative of young B-type stars in the solar neighborhood, as can be seen from the comparison with the cosmic abundance standard (CAS) by Przybilla et al. (2008a); see the inset of Fig. 5. The differential abundance pattern of HIP 60350 relative to the reference star 18 Peg is shown in Fig. 5. The results obtained so far are

summarized in Table 1, while a detailed list of lines used for both spectroscopic investigations can be found in Table 2. From the latter, we conclude that our quantitative analysis is not affected by a systematic bias.

3. KINEMATIC ANALYSIS

The knowledge of proper motions provides access to the full 3D kinematics of HIP 60350 because distance and radial velocity are known (see above). In this work, we made use of the new reduction of the *Hipparcos* Catalog (van Leeuwen 2007), giving $\mu_\alpha \cos(\delta) = -13.51 \pm 1.31 \text{ mas yr}^{-1}$ and $\mu_\delta = 16.34 \pm 1.37 \text{ mas yr}^{-1}$. The VizieR database (Ochsenbein et al. 2000) lists five ground-based measurements that are in excellent agreement with the *Hipparcos* values. Consequently, the current space velocity relative to the LSR is $v_{\text{LSR}} = 407 \text{ km s}^{-1}$. This value transforms into a total Galactic rest frame velocity of $v_{\text{grf}} = 530 \pm 35 \text{ km s}^{-1}$, slightly exceeding the

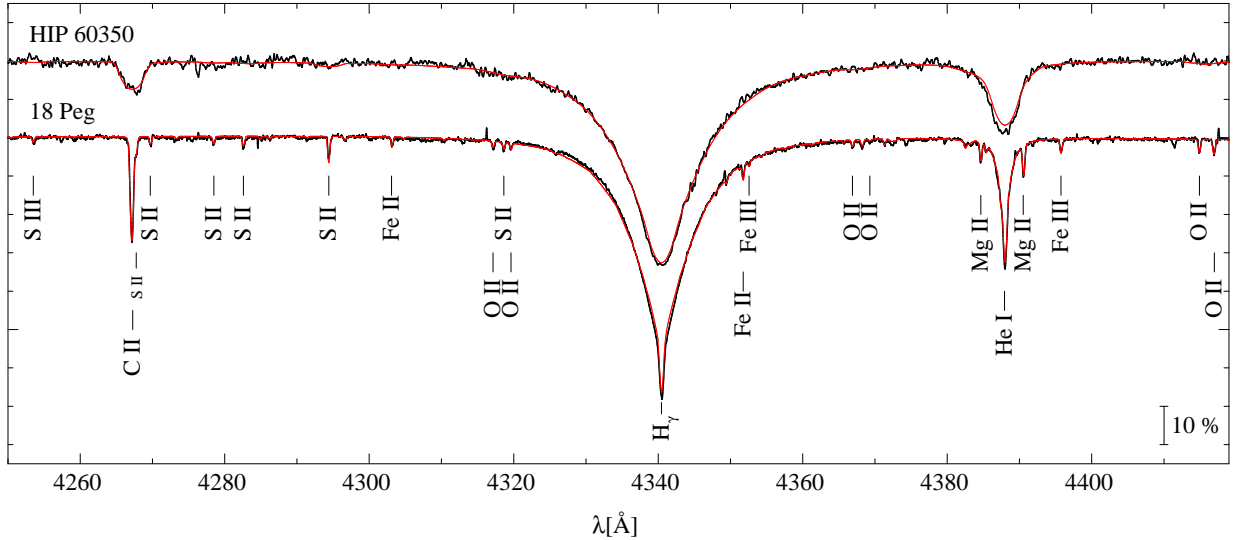


FIG. 2.— Comparison of final spectrum synthesis for HIP 60350/18 Peg (red line) with normalized HET/FOCES observation (black line) for an exemplary region around H_γ .

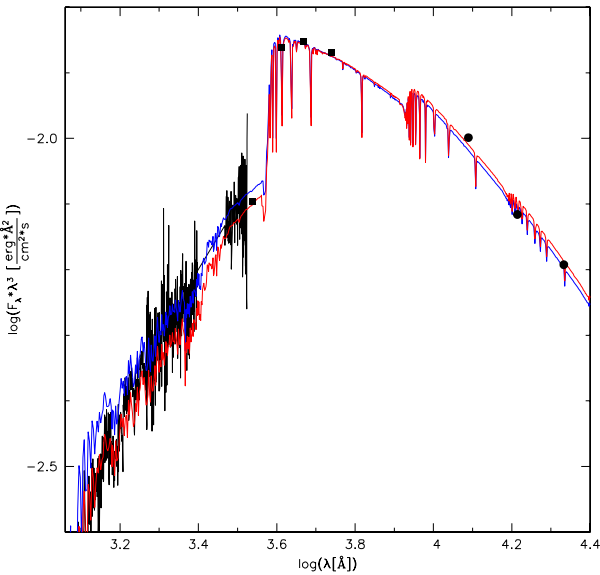


FIG. 3.— Observed SED from low-resolution IUE UV-spectro- (black line), *uvby*- (black filled squares; Tobin 1985) and *JHK*-photometry (black filled circles, Cutri et al. 2003). The measurements are plotted vs. two different ATLAS9 models. The red one, calculated for the parameters of Table 1 (helium enriched), obviously fits better than the blue one, which is the best model assuming a standard solar helium abundance ($T_{\text{eff}} = 16900$ K, $\log(g [\text{cm s}^{-2}]) = 4.18$). Interstellar extinction was corrected by using a color excess of $E(B - V) = 0.023$ mag according to Schlegel et al. (1998).

Milky Way's local escape velocity $v_{\text{esc}} = 522 \text{ km s}^{-1}$ derived from the Galactic gravitational potential of Allen & Santillan (1991). Hence a detailed kinematic study seemed worthwhile.

To do so, the Galactic potential of Allen & Santillan as well as the numerical code of Odenkirchen & Brosche (1992) was applied. This allowed the stellar orbit to be traced back to the Galactic plane to investigate whether HIP 60350 is a runaway star at all and to determine the flight time T_{flight} . Uncertainties were constrained via a Monte Carlo method that simultaneously and independently varied the initial parameters (i.e., the components of position and velocity), assuming for each a Gaussian

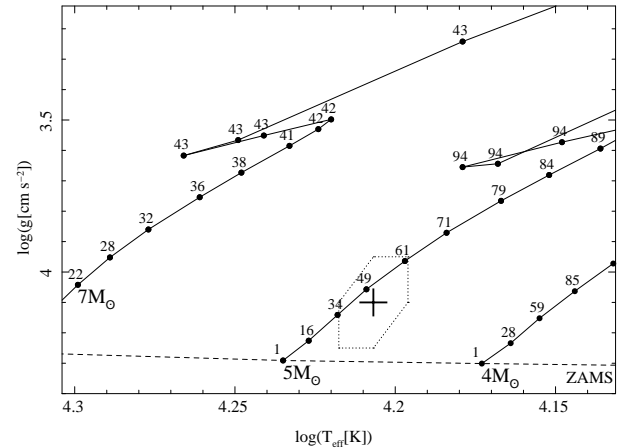


FIG. 4.— Position of HIP 60350 in a $(T_{\text{eff}}, \log g)$ diagram with evolution tracks calculated by Schaller et al. (1992). Time steps are marked by filled circles giving the age in Myr. Uncertainties are indicated by the dotted hexagon. The locus of the ZAMS is displayed as well.

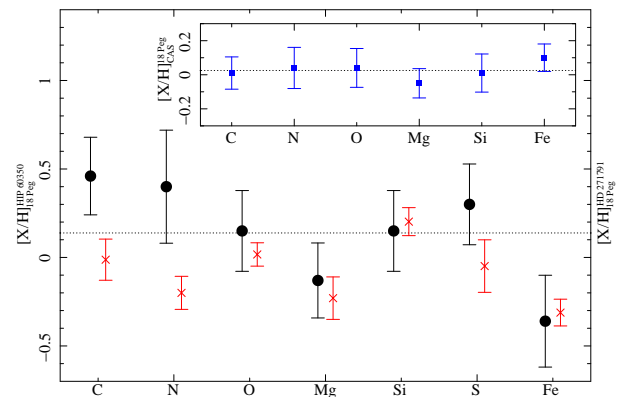


FIG. 5.— Metal abundances of HIP 60350 (black filled circles) and HD 271791 (red crosses, Przybilla et al. 2008b) relative to the reference star 18 Peg. We use the notation $[X/H]_{\text{A}}^{\text{B}} \equiv \log(X/H)_{\text{A}} - \log(X/H)_{\text{B}}$. The inset shows the abundances of 18 Peg (blue filled squares) relative to the CAS by Przybilla et al. (2008a) revealing that 18 Peg is representative of the solar neighborhood. The dotted lines mark the average of the filled circles or squares, respectively.

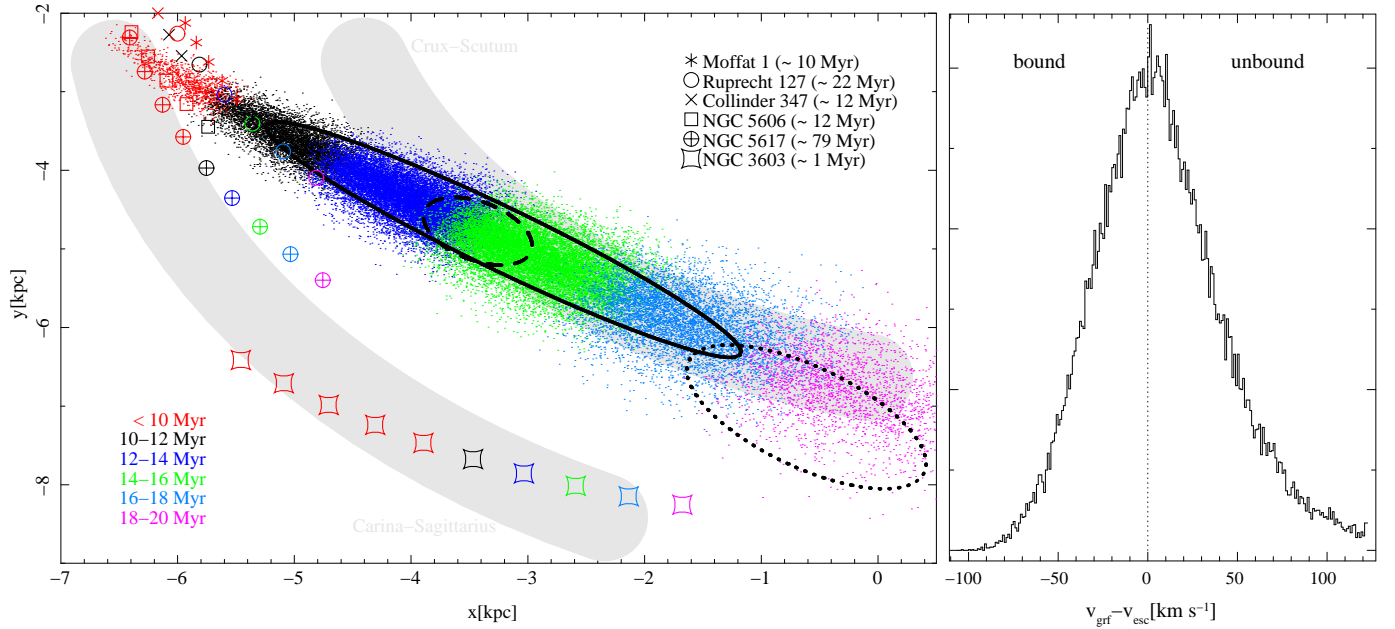


FIG. 6.— Left panel: Galactic disk intersection region of the sample of orbits (dots). Additionally, the trajectories of the best open cluster candidates are depicted using data from Dias et al. (2002). The flight time’s color code is given in the lower left corner. A right-handed, non-rotating frame of reference with the Galactic center at the origin, Galactic north pole in the positive z -direction and the Sun’s current position $(-8.0, 0, 0)$ kpc is used. The ellipses mark the 1σ region with (solid) or without (dashed, dotted) accounting for uncertainties in distance, respectively, whereby the last one is the result of our computation based on the data from Tenjes et al. (2001). The gray-shaded regions schematically represent the locus of two spiral arms 14 Myr ago. Right panel: histogram showing the distribution of (un)bound trajectories in the sample. The abscissa is the difference between current space velocity v_{grf} and the local escape velocity v_{esc} according to the potential of Allen & Santillan (1991).

distribution. The following results are average or – when explicitly noted – median values of a sample of 50 000 trajectories. Uncertainties are expressed by the standard deviation.

The obtained travel time $T_{\text{flight}} = 14 \pm 3$ Myr is shorter than the evolutionary timescale $T_{\text{evol}} = 45_{-30}^{+15}$ Myr and hence consistent with a runaway nature of the star⁸. To clarify the question whether HIP 60350 is bound to the Galaxy or not, we compared the current space and local escape velocity for each of our sample’s orbits (see the right panel of Fig. 6) showing that more than half of the trajectories (median value for $v_{\text{grf}} - v_{\text{esc}}$: 5 km s^{-1}) computed for HIP 60350 are unbound to the Milky Way. Considering Galactic gravitational potentials with a lower (Xue et al. 2008) or larger (Abadi et al. 2009) dark matter halo mass yields an overwhelming majority of unbound or bound orbits, respectively.

The disk intersection points of our sample of orbits are depicted in the left panel of Fig. 6 and imply an origin in the Galactic plane 6.1 ± 0.6 kpc away from the Galactic center, excluding a SMBH and hence the Hills mechanism as ejection scenario. The solid ellipse marks the 1σ region, i.e., it contains about 68% of all points. The dashed 1σ ellipse is the result of a calculation without taking variations of position into account and is intended to show the dramatic effects of the distance uncertainty. The latter is to be compared to the dotted 1σ ellipse, which is our result when reproducing the conditions given in Tenjes et al. (2001); see Sect. 4.2. In addition, the figure schematically shows the locus of the two Galactic spiral arms Carina-Sagittarius and Crux-Scutum 14

Myr ago as gray-shaded areas, indicating that the star originated in or near the latter. Their positions were estimated from the polynomial logarithmic arm model of Hou et al. (2009) and the Galactic rotation curve of Allen & Santillan (1991).

Our calculations also allowed the distribution of ejection velocities v_{ej} to be examined, defined as the absolute velocity at disk intersection relative to the rotating Galactic rest frame, yielding a median of 379 km s^{-1} or an average of $389 \pm 43 \text{ km s}^{-1}$, respectively.

4. DISCUSSION

According to the results of Sect. 3, HIP 60350 clearly qualifies as a candidate hyper-runaway star, i.e., an unbound runaway star. It has an ejection velocity similar to HD 271791 ($v_{\text{ej}} \approx 400 \text{ km s}^{-1}$; Przybilla et al. 2008b), the first discovered hyper-runaway star, and was also expelled in the direction of Galactic rotation to reach its extreme current space velocity. Neither of the two ejection mechanisms – binary supernova explosion and dynamical interaction – can be strictly confirmed nor rejected for HIP 60350.

4.1. Supernova explosion in a binary system

Various recent measurements of the Galactic metallicity gradient (e.g., Daflon & Cunha 2004) show a large scatter of abundances for individual stars. Hence, the low iron abundance of Table 1 may not be in contradiction to the star’s birthplace ~ 6 kpc away from the Galactic center and may in fact represent HIP 60350’s baseline metallicity. On that condition, Fig. 5 reveals an enhancement of α -elements resembling that of HD 271791 and thus giving indication for a supernova ejection event. Therefore, an analogous scenario as for HD 271791 can be devised

⁸ For comparison, Tenjes et al. (2001) derive $T_{\text{flight}} = 20.4$ Myr while Maitzen et al. (1998) give $T_{\text{evol}} \approx 15$ Myr.

(see Przybilla et al. 2008b for details). In brief, together with a primary star of at least $25 M_{\odot}$ on the zero-age main sequence (ZAMS), HIP 60350 formed a binary system that underwent a common-envelope phase. The resulting viscous forces triggered the spiraling in of the secondary component until the primary's shell was expelled due to the deposition of orbital energy by the secondary, leaving the primary behind as a Wolf-Rayet star. Eventually, the resulting very close binary system was disrupted by the primary's supernova explosion releasing HIP 60350 at almost orbital velocity. Considering a $15 M_{\odot}$ Wolf-Rayet star and making typical assumptions (synchronization of orbital and rotational periods/axes of the runaway star, circular orbits, symmetric supernova explosion to relate orbital and ejection velocity according to Tauris & Takens 1998, $1.4 M_{\odot}$ supernova remnant) a pre-supernova system, with separation $\sim 11 R_{\odot}$ and period ~ 0.9 days that is consistent with all observational constraints can be constructed. Requiring the Wolf-Rayet star to be of subclass WN could account for HIP 60350's high helium and nitrogen abundances.

4.2. Dynamical interaction in star clusters

Alternatively, Fig. 5 can be interpreted to show a metallicity slightly exceeding that of 18 Peg as well as the CAS. This is consistent with the kinematically predicted birthplace of Sect. 3, in particular as HIP 60350's iron abundance is deduced from a line which gives the lowest value for the reference star (see Table 2). In that case, a dynamical ejection from a star cluster may be more likely. Knowing the flight time to the Galactic plane and the corresponding intersection region, we searched the catalog of open clusters by Dias et al. (2002) for objects that match in position at the respective travel time as well as evolutionary age. For our star we found at least five appropriate candidates (see the left panel of Fig. 6): Ruprecht 127 (age in Myr: ~ 22), NGC 5606 (~ 12), NGC 5617 (~ 79), Collinder 347 (~ 12) and Mofat 1 (~ 10). The vicinity of the current massive cluster NGC 3603 has been suggested as the possible spatial origin by Tenjes et al. (2001), but we find it not to be suited because its trajectory is far from the Galactic plane inter-

section area of HIP 60350. Note that the catalog contains full 3D velocity information for the first three objects while all others were assumed to move on circular orbits around the Galactic center. It is important to mention that accounting for errors in the cluster trajectories analogously to the stellar orbit would noticeably increase the overlapping regions. Furthermore, many promising candidates, e.g., located in the Crux-Scutum spiral arm of the Milky Way, are very likely obscured by interstellar extinction and hence have not yet been discovered as already stated by Tenjes et al. (2001). The supersolar helium abundance of HIP 60350 might be the consequence of a merger event that occurred in the course of the dynamical ejection (see Leonard 1995).

5. SUMMARY

To summarize, based on a detailed spectroscopic and kinematic study we were able to significantly refine the stellar parameters, distance and possible place of birth of HIP 60350 revealing clear indications for a hyper-runaway nature of the star. Additionally, elemental abundances were derived via a NLTE analysis allowing the two competing ejection mechanisms of the runaway star, supernova explosion or dynamical interaction, to be discussed based on information previously not at hand. Performing this kind of investigation on optical spectra with a higher S/N than currently available might finally constrain HIP 60350's origin unambiguously.

We thank S. Müller and T. Kupfer for taking the TWIN spectra, H. Edelmann for support with the reduction of the HET data, H. Hirsch for providing access to his spectrum analyzing software SPAS and M. Firnstein for various pieces of advice, especially concerning the use of SPAS. Travel to the DSAZ (Calar Alto, Spain) was supported by the Deutsche Forschungsgemeinschaft (DFG) under grants He1356/50-1 and He1356/52-1. Publication costs were partly covered by DFG (grant He1356/45-1). *Facilities:* HET (HRS), CAO:3.5m (TWIN), CAO:2.2m (FOCES), IUE

REFERENCES

- Abadi, M. G., Navarro, J. F., & Steinmetz, M. 2009, *ApJ*, 691, L63
- Allen, C., & Santillan, A. 1991, *RevMexAA*, 22, 255
- Becker, S. R., & Butler, K. 1989, *A&A*, 209, 244
- Blaauw, A. 1961, *Bull. Astron. Inst. Netherlands*, 15, 265
- Brown, W. R., Geller, M. J., Kenyon, S. J., & Kurtz, M. J. 2005, *ApJ*, 622, L33
- Butler, K., & Giddings, J. R. 1985, in *Newsletter of Analysis of Astronomical Spectra*, No. 9 (London: Univ. London)
- Butler, K., Mendoza, C., & Zeppen, C. J. 1993, *J. Phys. B*, 26, 4409
- Cutri, R. M., et al. 2003, 2MASS All Sky Catalog of Point Sources (The IRSA 2MASS All-Sky Point Source Catalog, NASA/IPAC Infrared Science Archive), <http://irsa.ipac.caltech.edu/applications/Gator/>
- Dafon, S., & Cunha, K. 2004, *ApJ*, 617, 1115
- de Boer, K. S., Richtler, T., & Heber, U. 1988, *A&A*, 202, 113
- Dias, W. S., Alessi, B. S., Moitinho, A., & Lépine, J. R. D. 2002, *A&A*, 389, 871
- Edelmann, H., Napiwotzki, R., Heber, U., Christlieb, N., & Reimers, D. 2005, *ApJ*, 634, L181
- Froese Fischer, C., & Tachiev, G. 2004, *At. Data Nucl. Data Tables*, 87, 1
- Froese Fischer, C., Tachiev, G., & Irimia, A. 2006, *At. Data Nucl. Data Tables*, 92, 607
- Fuhr, J. R., Martin, G. A., & Wiese, W. L. 1988, *J. Phys. Chem. Ref. Data*, Vol. 17, Suppl. 4 (New York: American Institute of Physics and American Chemical Society)
- Fuhr, J. R., & Wiese, W. L. 1998, in *CRC Handbook of Chemistry and Physics*, ed. D. R. Lide (79th ed.; Boca Raton, FL: CRC Press)
- Giddings, J. R. 1981, PhD thesis, Univ. London
- Heber, U., Edelmann, H., Napiwotzki, R., Altmann, M., & Scholz, R.-D. 2008, *A&A*, 483, L21
- Hills, J. G. 1988, *Nature*, 331, 687
- Hirsch, H. A., Heber, U., O'Toole, S. J., & Bresolin, F. 2005, *A&A*, 444, L61
- Hou, L. G., Han, J. L., & Shi, W. B. 2009, *A&A*, 499, 473
- Kurucz, R. L. 1993, CD-ROM 13 (Cambridge: SAO)
- Kurucz, R. L., & Bell, B. 1995, Kurucz CD-ROM No. 23 (Cambridge, MA: Smithsonian Astrophysical Observatory)
- Leonard, P. J. T. 1995, *MNRAS*, 277, 1080
- Leonard, P. J. T., & Duncan, M. J. 1988, *AJ*, 96, 222
- Maitzen, H. M., Paunzen, E., Pressberger, R., Slettebak, A., & Wagner, R. M. 1998, *A&A*, 339, 782

- Mar, S., Pérez, C., González, V. R., Gigosos, M. A., del Val, J. A., de la Rosa, I., & Aparicio, J. A. 2000, *A&AS*, 144, 509
- Matheron, P., Escarguel, A., Redon, R., Lesage, A., & Richou, J. 2001, *J. Quant. Spectrosc. Radiat. Transf.* 69, 535
- Mendoza, C., Eissner, W., LeDourneuf, M., & Zeippen, C. J. 1995, *J. Phys. B: At. Mol. Opt. Phys.* 28, 3485
- Nahar, S. N. 2002, *At. Data Nucl. Data Tables*, 80, 205
- Nieva, M. F., & Przybilla, N. 2006, *ApJ*, 639, L39
- Nieva, M. F., & Przybilla, N. 2007, *A&A*, 467, 295
- Nieva, M. F., & Przybilla, N. 2008, *A&A*, 481, 199
- Nussbaumer, H. 1986, *A&A*, 155, 205
- Ochsenbein, F., Bauer, P., & Marcout, J. 2000, *A&AS*, 143, 23
- Odenkirchen, M., & Brosche, P. 1992, *Astron. Nachr.*, 313, 69
- Pfeiffer, M. J., Frank, C., Baumüller, D., Fuhrmann, K., & Gehren, T. 1998, *A&AS*, 130, 381
- Poveda, A., Ruiz, J., & Allen, C. 1967, *Bol. Obs. Tonantzintla Tacubaya*, 4, 86
- Przybilla, N., Butler, K., Becker, S. R., & Kudritzki, R. P. 2006, *A&A*, 445, 1099
- Przybilla, N., Nieva, M.-F., & Butler, K. 2008a, *ApJ*, 688, L103
- Przybilla, N., Nieva, M. F., Heber, U., & Butler, K. 2008b, *ApJ*, 684, L103
- Ramspeck, M., Heber, U., & Edelmann, H. 2001, *A&A*, 379, 235
- Schaller, G., Schaerer, D., Meynet, G., & Maeder, A. 1992, *A&AS*, 96, 269
- Schlegel, D. J., Finkbeiner, D. P., & Davis, M. 1998, *ApJ*, 500, 525
- Tauris, T. M., & Takens, R. J. 1998, *A&A*, 330, 1047
- Tenjes, P., Einasto, J., Maitzen, H. M., & Zinnecker, H. 2001, *A&A*, 369, 530
- Tobin, W. 1985, *A&AS*, 60, 459
- Tobin, W. 1987, in *IAU Colloq. 95, The Second Conference on Faint Blue Stars*, ed. A. G. D. Philip, D. S. Hayes, & J. W. Liebert (Schenectady: L. Davis Press), 149
- van Leeuwen, F. 2007, *Astrophysics and Space Science Library* 350, *Hipparcos, the New Reduction of the Raw Data* (Berlin: Springer)
- Wiese, W. L., Fuhr, J. R., & Deters, T. M. 1996, *J. Phys. Chem. Ref. Data*, Mon. 7 (Washington, DC: American Chemical Society and American Institute of Physics)
- Wiese, W. L., Smith, M. W., & Miles, B. M. 1969, *Nat. Stand. Ref. Data Ser.*, 22 (Washington, DC: Nat. Bur. Stand. [U.S.]
- Xue, X. X., et al. 2008, *ApJ*, 684, 1143

TABLE 3
SPECTRAL LINE ANALYSIS OF HIP 60350 AND 18 PEG

$\lambda(\text{\AA})$	$\chi(\text{eV})$	$\log gf$	Accuracy	Source	$\log(X/H) + 12$	
					HIP 60350	18 Peg
C II:						
3918.98	16.33	-0.533	B	WFD	...	8.19
3920.69	16.33	-0.232	B	WFD	...	8.30
4267.00	18.05	0.563	C+	WFD	8.69	8.19
4267.26	18.05	0.716	C+	WFD	-"-	-"-
4267.26	18.05	-0.584	C+	WFD	-"-	-"-
5132.94	20.70	-0.211	B	WFD	8.93	8.37
5133.28	20.70	-0.178	B	WFD	-"-	-"-
5145.16	20.71	0.189	B	WFD	8.73	8.34
5151.09	20.71	-0.179	B	WFD	...	8.39
5662.47	20.71	-0.249	B	WFD	...	8.41
6578.05	14.45	-0.087	C+	N02	...	8.25
6582.88	14.45	-0.388	C+	N02	...	8.37
6783.90	20.71	0.304	B	WFD	...	8.44
					8.79	8.33
					± 0.13	± 0.09
N II:						
3995.00	18.50	0.163	B	FFT	8.22	7.72
4035.08	23.12	0.599	B	BB89	...	7.87
4041.31	23.14	0.748	B	MAR	...	7.90
4176.16	23.20	0.316	B	MAR	...	7.88
4227.74	21.60	-0.060	B	WFD	...	7.94
4236.91	23.24	0.383	X	KB	...	7.74
4237.05	23.24	0.553	X	KB	...	-"-
4241.76	23.24	0.210	X	KB	...	7.59
4241.79	23.25	0.713	X	KB	...	-"-
4447.03	20.41	0.221	B	FFT	...	7.85
4601.48	18.47	-0.452	B+	FFT	8.65	7.88
4607.16	18.46	-0.522	B+	FFT	...	7.74
4630.54	18.48	0.080	B+	FFT	...	7.70
4643.08	18.48	-0.371	B+	FFT	...	7.83
5001.13	20.65	0.257	B	FFT	...	7.91
5001.48	20.65	0.435	B	FFT	...	-"-
5005.15	20.67	0.587	B	FFT	...	7.84
5045.10	18.48	-0.407	B+	WFD	...	7.68
5666.63	18.47	-0.104	B+	MAR	7.97	7.67
5676.02	18.46	-0.356	B+	MAR	7.96	7.66
5679.56	18.48	0.221	B+	MAR	-"-	7.93
					8.20	7.80
					± 0.32	± 0.11
O I:						
6155.96	10.74	-1.363	B+	WFD	8.98	8.81
6155.97	10.74	-1.011	B+	WFD	-"-	-"-
6155.99	10.74	-1.120	B+	WFD	-"-	-"-
6156.74	10.74	-1.487	B+	WFD	-"-	-"-
6156.76	10.74	-0.898	B+	WFD	-"-	-"-
6156.78	10.74	-0.694	B+	WFD	-"-	-"-
6158.15	10.74	-1.841	B+	WFD	-"-	8.81
6158.17	10.74	-0.995	B+	WFD	-"-	-"-
6158.19	10.74	-0.409	B+	WFD	-"-	-"-
7771.94	9.15	0.354	A	FFT	8.91	8.54
7774.17	9.15	0.207	A	FFT	-"-	8.75
7775.39	9.15	-0.015	A	FFT	-"-	8.68
					8.95	8.72
					± 0.05	± 0.11
O II:						
3911.96	25.66	-0.014	B+	FFT	...	8.93
3912.12	25.66	-0.907	B+	FFT	...	-"-
4069.62	25.63	0.144	B+	FFT	...	8.81
4069.88	25.64	0.352	B+	FFT	...	-"-
4072.72	25.65	0.528	B+	FFT	...	8.88
4075.86	25.67	0.693	B+	FFT	...	8.94
4185.45	28.36	0.604	D	WFD	...	8.75
4317.14	22.97	-0.368	B+	FFT	...	8.86
4319.63	22.98	-0.372	B+	FFT	...	8.69
4366.89	23.00	-0.333	B+	FFT	...	8.73
4369.28	26.23	-0.383	B+	FFT	...	8.88
4414.90	23.44	0.207	B	FFT	...	8.63
4416.97	23.42	-0.043	B	FFT	...	8.95
4452.38	23.44	-0.767	B	FFT	...	8.84
4590.97	25.66	0.331	B+	FFT	...	8.91

TABLE 3
SPECTRAL LINE ANALYSIS OF HIP 60350 AND 18 PEG

4661.63	22.98	-0.269	B+	FFT	...	8.73
4699.22	26.23	0.238	B	FFT	...	8.88
4705.35	26.25	0.533	B	FFT	...	8.78
					...	8.82
					...	±0.10
Mg II:						
4384.64	10.00	-0.792	B+	FW	...	7.56
4390.51	10.00	-1.703	D	FW	...	7.54
4390.57	10.00	-0.530	B+	FW	...	- ⁿ -
4433.99	10.00	-0.900	C+	FW	...	7.53
4481.13	8.86	0.730	B+	FW	7.38	7.41
4481.15	8.86	-0.570	B+	FW	- ⁿ -	- ⁿ -
4481.33	8.86	0.575	B+	FW	- ⁿ -	- ⁿ -
					7.38	7.51
					...	±0.07
Si II:						
4621.42	12.53	-0.608	D	MELZ	...	7.55
4621.70	12.53	-1.754	E	MELZ	...	- ⁿ -
4621.72	12.53	-0.453	D	MELZ	...	- ⁿ -
5041.02	10.07	0.029	B	MERLR	7.72	7.34
5055.98	10.07	0.523	B	MERLR	...	7.43
5056.32	10.07	-0.492	B	MERLR	...	- ⁿ -
5185.54	12.84	-0.059	D	MELZ	...	7.59
5978.93	10.07	-0.06	D	WSM	...	7.35
6347.11	8.12	0.177	B+	FFTI	7.71	7.61
6371.37	8.12	-0.126	B	FFTI	7.63	7.44
					7.69	7.47
					±0.05	±0.11
Si III:						
4552.62	19.02	0.292	B+	FFTI	...	7.61
4567.84	19.02	0.068	B+	FFTI	7.52	7.48
4574.76	19.02	-0.409	B	FFTI	7.73	7.49
4813.33	25.98	0.708	B+	BMZ	...	7.61
5739.73	19.72	-0.096	B+	FFTI,N86	...	7.64
					7.62	7.57
					±0.15	±0.08
S II:						
3990.91	15.90	-0.30	E	WSM	...	7.24
3998.76	15.87	0.06	E	FW	...	7.17
4028.75	15.90	-0.00	D	FW	...	7.20
4032.76	16.25	0.24	D	FW	...	7.07
4153.06	15.90	0.62	D	FW	7.49	7.08
4162.66	15.94	0.78	D	FW	7.31	6.98
4168.38	15.87	-0.16	E	WSM	...	7.10
4189.68	15.90	-0.05	E	FW	...	7.13
4217.18	15.94	-0.15	E	WSM	...	7.07
4217.30	14.85	-1.479	B	FFTI	...	- ⁿ -
4267.76	16.10	0.29	E	FW	...	7.19
4269.72	16.09	-0.12	E	WSM	...	7.11
4278.50	16.09	-0.11	E	FW	...	7.07
4282.59	16.10	-0.01	E	WSM	...	7.16
4294.40	16.13	0.58	D	FW	...	6.95
4318.64	16.13	-0.08	E	WSM	...	7.22
4524.67	15.07	-0.744	B	FFTI	...	6.92
4524.94	15.07	0.032	B	FFTI	...	6.92
4656.75	13.58	-0.827	B	FFTI	...	7.25
4716.27	13.62	-0.366	B	FFTI	...	7.16
4815.55	13.67	0.068	B	FFTI	7.56	6.99
4917.19	14.00	-0.375	B	FFTI	...	7.24
4942.47	13.58	-1.034	B	FFTI	...	7.15
5009.56	13.62	-0.235	B	FFTI	...	7.11
5014.04	14.07	0.046	B	FFTI	...	7.12
5027.20	13.09	-0.664	B	FFTI	...	7.07
5032.43	13.67	0.187	B	FFTI	7.15	6.93
5142.32	13.15	-1.004	B	FFTI	...	7.00
5201.03	15.07	0.088	B	FFTI	7.55	6.97
5201.37	15.07	-0.712	B	FFTI	- ⁿ -	- ⁿ -
5212.27	15.07	-1.444	B	FFTI	...	6.99
5212.62	15.07	0.316	B	FFTI	...	- ⁿ -
5320.72	15.07	0.431	B	FFTI	...	6.96
5345.71	15.07	0.289	B	FFTI	7.22	6.98
5346.08	15.07	-1.161	B	FFTI	- ⁿ -	6.96
5428.65	13.58	-0.175	B	FFTI	...	7.03

TABLE 3
SPECTRAL LINE ANALYSIS OF HIP 60350 AND 18 PEG

5432.79	13.62	0.205	B	FFTI	...	7.01
5453.85	13.67	0.442	B	FFTI	...	6.92
5473.61	13.58	-0.226	B	FFTI	...	7.05
5509.70	13.62	-0.175	B	FFTI	7.3	7.08
5526.24	13.70	-0.871	B	FFTI	...	6.90
5564.95	13.67	-0.335	B	FFTI	...	7.09
5578.87	13.68	-0.727	B	FFTI	...	7.10
5606.15	13.73	0.123	B	FFTI	7.44	6.89
5616.63	13.66	-0.845	B	FFTI	...	7.19
5647.02	14.00	0.021	B	FFTI	7.56	7.20
5660.00	13.68	-0.220	B	FFTI	7.23	7.02
5664.77	13.66	-0.426	B	FFTI	- ^p -	7.11
5819.25	14.07	-0.713	B	FFTI	...	7.26
6286.34	14.16	-0.750	B	FFTI	...	7.11
6286.94	14.29	-0.157	B	FFTI	...	- ^p -
6384.89	14.16	-0.695	B	FFTI	...	7.29
6397.35	14.16	-0.434	B	FFTI	...	7.25
					7.38	7.08
					±0.16	±0.11
S III:						
4253.50	18.24	0.095	B	FFTI	...	7.02
Fe II:						
4178.86	2.58	-2.48	C	FMW	...	7.59
4233.17	2.58	-2.00	C	FMW	...	7.62
4303.17	2.70	-2.49	C	FMW	...	7.59
4351.76	2.70	-2.10	C	FMW	...	7.44
4508.28	2.86	-2.31	D	KB	...	7.52
4515.34	2.84	-2.48	D	FMW	...	7.50
4520.22	2.81	-2.60	D	FMW	...	7.56
4522.63	2.84	-2.11	C	KB	...	7.50
4549.47	2.82	-1.75	C	FMW	...	7.49
4555.75	2.83	-2.32	D	KB	...	7.56
4576.34	2.84	-3.04	D	FMW	...	7.59
4582.83	2.84	-3.10	C	FMW	...	7.63
4583.83	2.81	-2.02	D	FMW	...	7.65
4629.33	2.81	-2.37	D	FMW	...	7.53
4923.92	2.89	-1.32	C	FMW	...	7.58
5018.44	2.89	-1.22	C	FMW	7.18	7.42
5197.57	3.23	-2.23	C	KB	...	7.63
5234.62	3.22	-2.15	C	KB	...	7.67
5316.61	3.15	-1.85	C	FMW	...	7.62
					7.18	7.56
					...	±0.07
Fe III:						
4352.57	8.25	-2.870	X	KB	...	7.48
4395.75	8.26	-2.595	X	KB	...	7.52
4431.02	8.25	-2.572	X	KB	...	7.50
5073.90	8.65	-2.557	X	KB	...	7.52
5086.70	8.66	-2.590	X	KB	...	7.59
5127.39	8.66	-2.218	X	KB	...	7.43
5127.63	8.66	-2.564	X	KB	...	- ^p -
5156.11	8.64	-2.018	X	KB	...	7.41
					...	7.49
					...	±0.06